Temporal Characteristics of P-band Tomographic Radar Backscatter of a Boreal Forest

Citation for the original published paper (version of record):
Monteith, A., Ulander, L. (2021)
Temporal Characteristics of P-band Tomographic Radar Backscatter of a Boreal Forest
IEEE Journal of Selected Topics in Applied Earth Observations and Remote Sensing, 14: 1967-1984
http://dx.doi.org/10.1109/JSTARS.2021.3050611

Temporal Characteristics of P-band Tomographic Radar Backscatter of a Boreal Forest

Albert R. Monteith, *Student Member, IEEE* and Lars M. H. Ulander, *Fellow, IEEE,*

***Abstract*—Temporal variations in synthetic aperture radar (SAR) backscatter over forests are of concern for any SAR mission with the goal of estimating forest parameters from SAR data. In this article, a densely sampled, two-year long time series of P-band (420 to 450 MHz) boreal forest backscatter, acquired by a tower-based radar, is analyzed. The experimental setup provides time series data at multiple polarizations. Tomographic capabilities allow the separation of backscatter at different heights within the forest. Temporal variations of these multi-polarimetric, tomographic radar observations are characterized and quantified. The mechanisms studied are seasonal variations, effects of freezing conditions, diurnal variations, effects of wind and the effects of rainfall on backscatter. An emphasis is placed on upper-canopy backscatter, which has been shown to be a robust proxy for forest biomass. The canopy backscatter was most sensitive to freezing conditions but was more stable than ground-level backscatter and full-forest backscatter during non-frozen conditions. The analysis connects tree water transport mechanisms and P-band radar backscatter for the first time. The presented results are useful for designing boreal forest parameter estimation algorithms, using data from P-band SARs, that are robust to temporal variations in backscatter. The results also present new forest remote sensing opportunities using P-band radars.**

***Index Terms*—Backscatter, boreal forest, P-band, time series.**

I. Introduction

FOREST backscatter measured using imaging radars varies with time due to changes in weather conditions and seasons [1]–[4]. If such variations are not accounted for, they may affect the accuracy of forest parameter estimates such as forest height and biomass, as estimated from synthetic aperture radar (SAR) data.

The European Space Agency's BIOMASS SAR satellite is scheduled for launch in 2021. The main scientific objective of the mission is to quantify forest carbon stocks and fluxes by estimating biomass from SAR observations [5], [6]. The BIOMASS SAR instrument will be the first ever spaceborne SAR operating at P-band (centered at 435 MHz). This relatively low frequency, compared to existing spaceborne SARs, allows the emitted electromagnetic waves to penetrate the canopy and reflect off larger structures such as branches and tree stems where the majority of a tree's biomass is located. This makes P-band especially sensitive to above-ground forest biomass [7]–[9]. A consequence of the increased canopy penetration is that the ground contributes significantly to the total backscattered field, either through direct rough surface scattering or double-bounce scattering by the ground and tree trunks [10]. Variations in ground roughness, slope and soil moisture can thus introduce a significant bias in the estimated biomass [11]. The BIOMASS mission is designed for fully-polarimetric, interferometric and tomographic imaging. In boreal forests, the combination of polarimetric channels in SAR observations have been shown to reduce the influence of the ground [12]. In tropical forests, tomographic intensity above 30 m above the ground was shown to be insensitive to topography and closely correlated with forest biomass [13]. Tomographic ground separation has also been achieved in boreal forests [14]. More recently, a ground-cancelling technique was developed whereby the ground contribution is suppressed by coherently combining interferometric image pairs, isolating the above-ground canopy contribution [15]. Central to all these biomass estimation approaches is the use of the measured backscatter, especially that of the above-ground canopy, to estimate biomass. Even with the ground component removed, the canopy backscatter does not uniquely depend on biomass. Changes in canopy backscatter due to weather and seasonal changes will affect the estimated biomass. Very little is known about the characteristics of such temporal variations, especially in boreal forests, making it difficult to design biomass estimation algorithms that are robust to temporal variations. The lack of a quantitative understanding of environmentally-induced backscatter variations is also the main issue in developing algorithms for forest degradation detection [11].

Forest backscatter observed by a SAR is governed by the geometry of forest structures (ground, stems, branches and leaves/needles) and the relative permittivities of these structures [16]. The geometry and permittivity determine the angular distribution and strength of these reflections as well as the absorption of electromagnetic energy in forest structures. Backscatter variations occur due to changes in either the geometry or permittivity of forest structures

Apart from tree growth, geometric changes occur mainly due to wind-induced tree swaying. The resulting displacement of scatterers is the on the order of microwave wavelengths, and thus affect the scattered field measured by a radar. To a lesser extent, terrestrial lidar observations have shown that geometric changes occur due to diurnal drooping and rising of branches [17]. Geometric changes therefore occur at timescales of seconds (wind) to years (tree growth).

An increase in the permittivity of the soil or vegetation

This work was financially supported by the Hildur and Sven Wingquist Foundation for Forest Research, the European Space Agency (ESA) and the Swedish National Space Agency.

Albert R. Monteith is with the Department of Space, Earth and Environment, Chalmers University of Technology, SE-412 96 Gothenburg, Sweden (e-mail: albert.monteith@chalmers.se).

Lars. M. H. Ulander is with the Department of Space, Earth and Environment, Chalmers University of Technology, SE-412 96 Gothenburg, Sweden, and also with the Radar Systems Unit, Swedish Defence Research Agency (FOI), SE-581 11 Linkping, Sweden (email: lars.ulander@chalmers.se).

increases the forest backscatter [18]. Changes in the permittivity of forest structures have been observed to be caused by a variety of mechanisms that affect the water content and chemical composition of forest materials [19]. A higher soil water content increases the permittivity of the soil and results in a stronger ground reflection [20]–[22]. Mechanisms driving water content variations in trees are significantly more complex. The most widely-accepted theory of water transport in trees is the cohesion-tension theory [23]. According to the cohesion-tension theory, water moves from the roots to the stomata (pores in leaves/needles for gas exchange with the atmosphere) as continuous columns of water as water is drawn out of stomata during transpiration. The flow of water from roots to stomata can be characterized by resistances, limiting the rate of upward flow, and capacitances, representing depletable water storages in the xylem (sapwood) and phloem (bark) [24], [25]. These water reserves are depleted in hot and dry conditions when the rate of transpiration exceeds soil water uptake, resulting in a change of permittivity of tree structures. The rate of transpiration is controlled by a complicated interaction between solar radiation, air temperature, relative humidity, air pressure, wind speed, CO_2 concentration, soil water availability and by the trees themselves through stomatal conductance [26], [27]. Intercepted precipitation increases the water content, which may increase the average permittivity of the canopy. In freezing conditions water freezes, resulting in a significant drop in permittivity. Reversible freezing occurs at different times, temperatures and rates in the various forest structures [28].

The mechanisms by which the permittivity of forest structures vary with time are complex and are currently not fully understood. Our lack of knowledge of how trees respond to their environment can be attributed to the laborious, indirect, invasive and even destructive nature of measurement techniques for quantifying spatio-temporal tree water content and chemical concentrations. The effects of changing weather and seasonal conditions on forest backscatter can currently only be revealed by empirical studies.

In this study, a boreal forest stand was observed using a tower-based multi-polarimetric, tomographic P-band radar. The aims of the study were to:

1) Collect densely-sampled time series of backscatter from different heights within the forest canopy
2) Identify the most significant temporal features in the dataset
3) Gain insight into the relationship between meteorological variables, backscatter and the underlying ecophysiological mechanisms

The goal of the experiment is to gain a better understanding of the electromagnetic scattering mechanisms taking place during SAR observations and how SAR observations are affected by changing weather and seasonal conditions.

First, the experiment is described in Section II and data analysis methods are detailed in Section III. Section IV contains the first analysis results of the dataset and a discussion of the results is given in Section V.

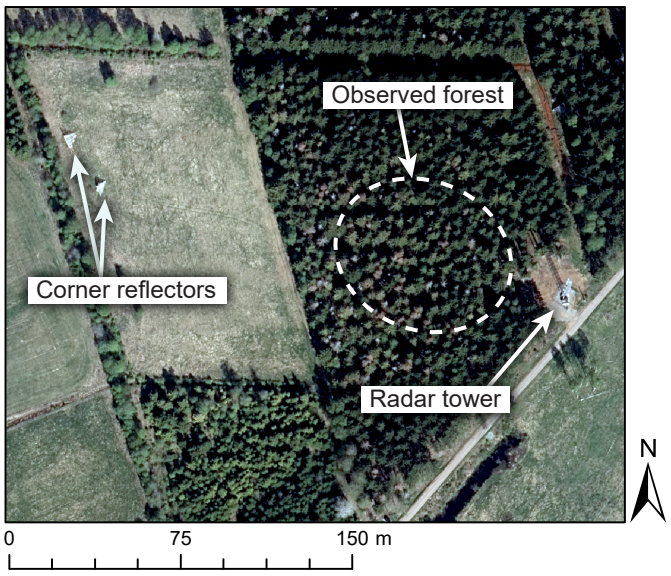

Fig. 1. RGB aerial photo of the experiment site acquired on 10 May 2018 by the Swedish National Land Survey (Lantmäteriet).

II. Experiment description

A. Experiment site

The observed forest is a homogeneous, mature stand of Norway spruce (*Picea abies* (L.) Karst). The 250 tons/ha biomass forest stand is located in the Remningstorp experimental forest in sourthern Sweden. The terrain is flat, is covered in moss and has little understory. The canopy height varies from 25 to 27 m. The 50 m-high radar tower is located at the edge of the forest stand (58° 27' 5" N, 13° 37' 35" E) as shown in Fig. 1. Several trihedral corner reflectors are placed around the site for calibration purposes.

B. Radar instrument

The BorealScat radar instrument consists of a vector network analyzer (VNA) connected to an antenna array. The VNA has 20 ports, each of which is connected to one of the 20 antennas in the array at the top of the tower (see Fig. 2). The VNA operates by transmitting, from a single VNA port, monochromatic pulses over a range of frequencies in discrete frequency steps. The stepped-frequency sweep covers a bandwidth of 30 MHz centered at 435 MHz. The signal is emitted in discrete frequency steps of 0.5 MHz. These signal parameters result in a range resolution of 5 m and a maximum unambiguous range of 300 m. The signal is emitted as an electromagnetic wave from a single antenna and scatters off the scene producing a scattered wave. The scattered wave is sampled in space by all 20 antennas in the array simultaneously. This parallel measurement configuration greatly reduces the measurement time compared to systems employing mechanical switching between antennas [29]. The antenna array was designed for tomographic imaging of the forest scene below at P-band to L-band (1270 MHz) for all linear polarization combinations (HH, VV, HV and VH). A second array is used for C-band (5410 MHz) measurements.

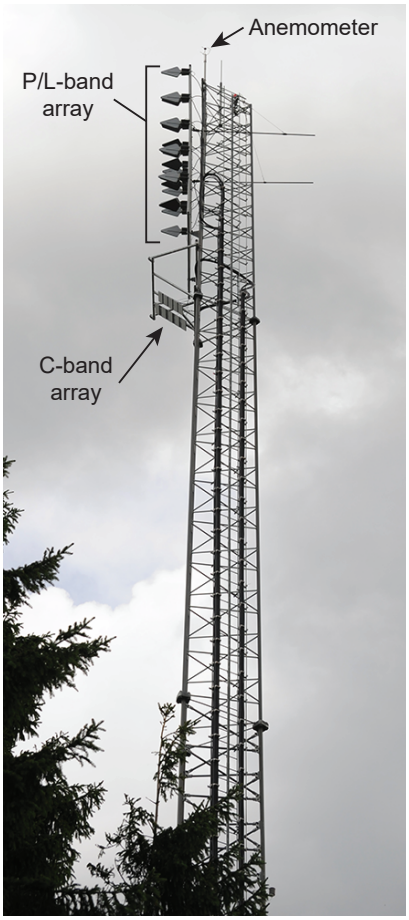

Fig. 2. Photo of the top section of the radar tower. The two antenna arrays are connected to the VNA on the ground via coaxial cables.

Details of the array designs are given in [29] and [30]. The antenna array geometry, VNA measurement characteristics and signal bandwidth result in mutual antenna coupling, which distorts the received signals. The mutual coupling component of the received signal is suppressed, without affecting the spatial resolution, using a novel procedure described in [31].

C. Radar measurement sequence

Tomographic image measurements are carried out in bursts of four measurements. The four measurements in a burst are separated by 5 s, and bursts are separated by 5 min (see Fig. 3). Each of the four measurements in a burst covers a tomographic measurement for each polarimetric combination (HH, HV, HH and VH). VV and HV measurements are done simultaneously. Likewise, HH and VH measurements are done simultaneously. This is possible because the VNA is capable of receiving signals from all 20 antennas in parallel. The measurement time for a single tomographic image is 40 ms, which is short enough for the forest scene to be assumed coherent during a tomographic measurement.

D. Meteorological observations

An on-site weather station measures air temperature, pressure and relative humidity at heights of 2 m and 30 m above ground. The 3D wind vector was measured by two ultrasonic anemometers installed at the top of the tower. Precipitation was measured by a heated rain gauge, which cannot distinguish between rain and snow. Soil temperature and volumetric water content were measured by time-domain reflectometry probes within the upper 30 cm of the soil.

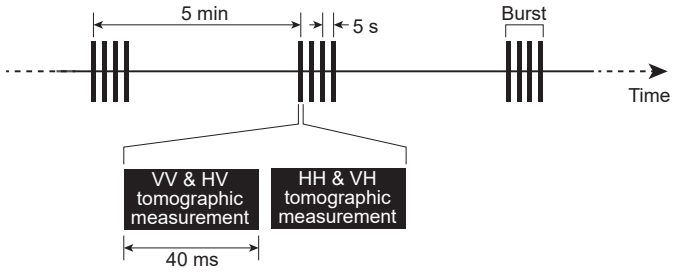

Fig. 3. Timeline of the measurement sequence. Every 5 minutes, a burst of four tomographic observations are made. Four tomograms for each polarization are thus acquired every 5 minutes.

Two surveillance cameras were installed on the tower to observe the state of snow on the canopy and ground. A photo was taken from each camera at 5 minute intervals, coinciding with the radar measurements. Snow depth and solar radiation were not measured during this study.

The water vapor pressure deficit (VPD), which is one of the drivers of transpiration, was estimated from the observed air temperature and relative humidity. The saturation pressure of water vapor, which is necessary for estimating the VPD, was estimated using the Goff-Gratch equation [32].

III. Method

A. Tomographic imaging

Tomographic SAR is based on multiple observations of the same scene. Radar observations acquired over a range of azimuth and elevation angles are coherently combined to construct a 3D distribution of the backscattered power [33]. This is typically implemented by multiple passes of an airborne or spaceborne radar with different incidence angles. The antenna array in this study has a vertical aperture, providing fine resolution in the ground range-height plane only. Tomographic images were formed in this plane. Azimuth resolution is determined by the antenna gain patterns, resulting in a variable resolution cell size throughout the image plane. This variable resolution cell size introduces a systematic gain which is dependent on the antenna gain patterns, antenna array geometry and signal parameters. This systematic gain was compensated for by normalizing the backscatter of each pixel by the energy of the image impulse response function for the respective pixel [31].

Tomographic images were constructed from the VNA measurements using a backprojection algorithm. To produce a focused tomographic image, it is necessary that the systematic phase differences between transmit-receive measurements contributing to the backprojection sum are small ($<$0.1 rad). Such phase, and also magnitude, imbalances were estimated and compensated for using a trihedral corner reflector as an external reference [31].

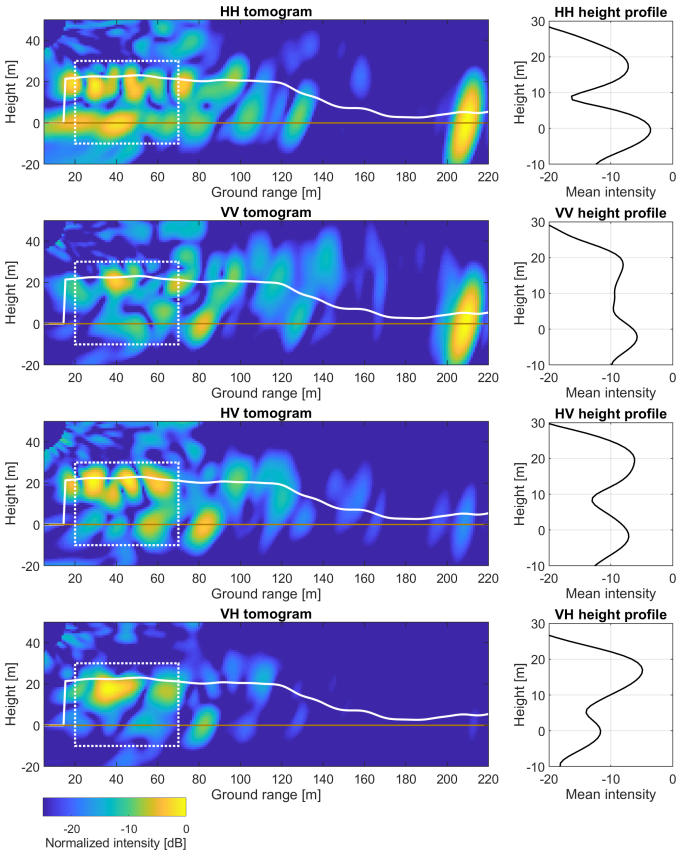

Fig. 4. Tomographic image examples from 06:00 on 1 September 2018. Height profiles of the image backscatter within the regions surrounded by dotted lines are shown on the right of each tomogram. Backscatter peaks at the ground level and upper canopy level. The solid white line shows a lidar-derived canopy height estimate and the brown line shows the ground level.

Examples of tomographic images are shown in Fig. 4. Each image exhibits speckle, which is a result of the coherent addition of scattering contributions from several elements within a resolution cell. The trihedral corner reflector lies on the ground at a ground range of 207 m, where the HH and VV tomograms show bright spots. The HV and VH images are different because different bistatic antenna pairs were used in the measurements. However, the trihedral corner reflector is also slightly visible in the HV image, which indicates that there is some cross-talk leakage for HV measurements. For this reason, the HV images were not analyzed in this study. VH images were included in this study, which would be equal to HV tomographic images for a monostatic radar, assuming target reciprocity.

The main forest region of interest (ROI) lies within a ground range of 20 to 70 m of the tower, covering similar incidence angles as space-borne SARs (20° to 55°). This region, indicated by the dotted rectangle in Fig. 4, is free from forest edges and corner reflectors. The forest reflectivity distribution for this region peaks at two heights for all polarizations: at the upper canopy (10 to 30 m height) and at the ground level (-10 to 10 m height). Reflections at the upper canopy level are mainly due to volume scattering and apparent reflections at the ground level are mainly due to the sum of direct ground scattering and double-bounce scattering (ground-trunk and trunk-ground) [14], [34]. These observations motivate a study of the backscatter mainly within these regions.

TABLE I
DEFINITION OF ROIS IN TOMOGRAPHIC IMAGES. THE NUMBER OF LOOKS FOR EACH ROI IS AN ESTIMATE ASSUMING FULLY-DEVELOPED SPECKLE.

ROI	Ground range interval	Height interval	Number of looks
Canopy	20 to 70 m	10 to 30 m	11.9
Ground	20 to 70 m	-10 to 10 m	8.6
Full forest	20 to 70 m	-10 to 30 m	18.6

B. Regions of interest

Temporal variation of backscatter in the tomographic images was studied using the mean intensities in three ROIs as defined in Table I. This was done to simplify the analysis of temporal variations by reducing the dimensionality of the data and, to obtain more accurate estimates of the backscatter. The ROIs are shown in Fig. 5 in the image plane. Estimation accuracy of the image backscatter must be improved by averaging over ROIs because the tomographic images exhibit speckle, whereby a large variance is associated with the backscatter estimate for a single pixel [35]. The backscatter within an ROI was averaged to yield a lower-variance estimate (higher number of looks) of the mean backscatter within the ROI. Table I lists the estimated number of looks for each ROI. These estimates were computed by simulating 1000 tomographic images of a cloud of uniformly-distributed point scatterers [31]. For each of the 1000 images, the mean backscatter over the three ROIs defined in Table I was estimated. These mean backscatter estimates were then used to estimate the equivalent number of looks [36]. In these estimates, fully-developed speckle was assumed, which is a reasonable assumption for forest canopies [35]. Even though the areas of the canopy and ground ROIs are the same, the estimated number of looks is lower for the ground region. This is because the resolution in elevation is slightly poorer closer to the ground compared to the canopy, which is a result of the antenna array geometry. To further increase the number of looks, the mean backscatter values from all four consecutive measurements in a burst (Fig. 3) were averaged. Under calm conditions, the four tomographic images are nearly identical, and thus no gain in the number of looks is achieved. In windy conditions, these four images will be different due to tree movement between image acquisitions, and the number of looks will be up to four times the estimates in Table I. The result is a multilooked backscatter time series for each polarization (HH, VV and VH) in each ROI (full forest, canopy and ground) with a sampling interval of 5 minutes. This procedure is illustrated in Fig. 6.

C. Time series

Six time series were analyzed: 3 polarizations (HH, VV and VH) for each of the three ROIs (canopy, ground and full forest). The time series exhibit variations at timescales of minutes (due to wind-induced movement) to years (due

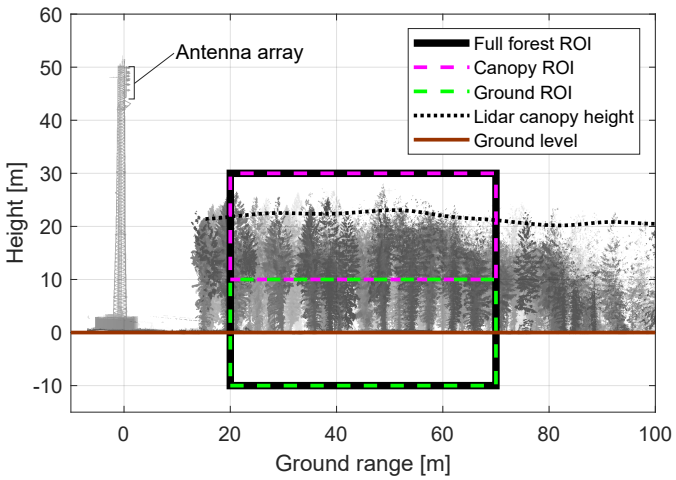

Fig. 5. Diagram (to scale) showing the three ROIs on the image plane in relation to the tower and forest geometry. The tower and forest visualization were produced by a terrestrial lidar scan in 2017 by the Swedish University of Agricultural Sciences (SLU). The canopy height estimate is the 99th percentile from an airborne lidar scan in 2014.

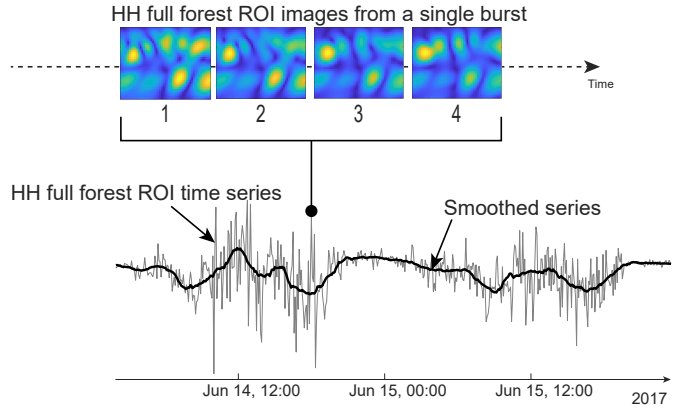

Fig. 6. Illustration of how time series were formed. The backscatter of four tomographic images was incoherently averaged to produce a single sample in a time series. The time series was further smoothed to reveal variations over longer timescales.

to seasons). The longer the timescale of interest, the more the time series must be temporally smoothed. For example, wind-induced variations obscure diurnal variations, so wind-induced variations must be smoothed to analyze diurnal variations (see Fig. 6). Smoothing of time series was done over different timescales, depending on the timescale of interest. The Savitzky-Golay filter was used to suppress short-term variations while preserving transients [37], which occur due to different mechanisms (e.g. rain).

To analyze diurnal variations, the diurnal components were extracted using a rank-1 approximation of the time series represented in matrix form, where each column corresponds to a different day [38]. All times in this article are local solar times (UTC+54.5 min for the site's longitude). In local solar times, the sun is highest in the sky at 12:00 every day. This is helpful when analyzing biological responses to diurnal variations in solar radiation.

The backscatter time series are not calibrated in an absolute manner. This means that the magnitude of backscatter variations over time are correct, but the time series have a constant, unknown offset from the true value. This is not a problem since only backscatter variations over time are of interest in this study.

IV. Results

A. Long-term variations

The temporally-smoothed backscatter from the full forest region of interest is shown in Fig. 7 for HH, VV and VH. The largest temporal variations in full forest backscatter occur during the winter when the air temperature drops below $0°$C, although the exact nature of freeze-thaw dynamics are not apparent from these curves. The freeze-thaw variations for HH and VV are similar, differing mainly in amplitude. HH variations during the winter (up to 8 dB) are larger than those of VV (up to 5 dB). Winter variations for VH (up to 10 dB) are larger than those of the co-pol channels. HH and VV show similar temporal dynamics throughout the rest of the observation period as well. Smaller variations over a range of approximately 3 dB at timescales of weeks can be observed for HH and VV during autumn 2017 and spring/summer 2018, which show some correlation with soil moisture. VH does not show long-term variations that are correlated with soil moisture. This is due to the stronger double-bounce scattering at HH and VV, which is affected by soil moisture. Despite the lack of sensitivity to soil moisture, VH full forest backscatter was no less stable than HH and VV during non-frozen conditions.

The temporally-smoothed backscatter from the ground ROI is shown in Fig. 8. The HH and VV ground-level backscatter time series are similar to those of the full-forest backscatter in Fig. 7. The ground-level backscatter dynamics for HH and VV are also similar to one another, showing some correlation with soil moisture content (Fig. 7) during non-frozen conditions. These observations confirm that the co-polarized backscatter variations are dominated by double-bounce scattering, which appears at the ground level. Soil moisture changes appears to be the dominant cause of long-term variations of the ground-level and full forest HH and VV backscatter during non-frozen conditions. The ground-level VH backscatter differs significantly from the full forest VH backscatter. This is because ground-level scattering, such as double-bounce scattering, is smaller for VH and therefore has little influence on the full forest VH backscatter. The ground-level VH backscatter shows some freeze-thaw effects, but otherwise erratic variations. These variations are amplified by the decibel scale since the ground-level backscatter is relatively low for VH due to significant attenuation by the canopy and little double-bounce scattering.

The temporally-smoothed backscatter from the canopy ROI is shown in Fig. 9. As before, the largest temporal variations in backscatter are seen during the winter for all polarizations. The freeze-thaw backscatter variations are largest for the canopy region, with more than 10 dB variations observed for all polarizations. During non-frozen conditions, the canopy backscatter is stable on the long term for all polarizations, especially

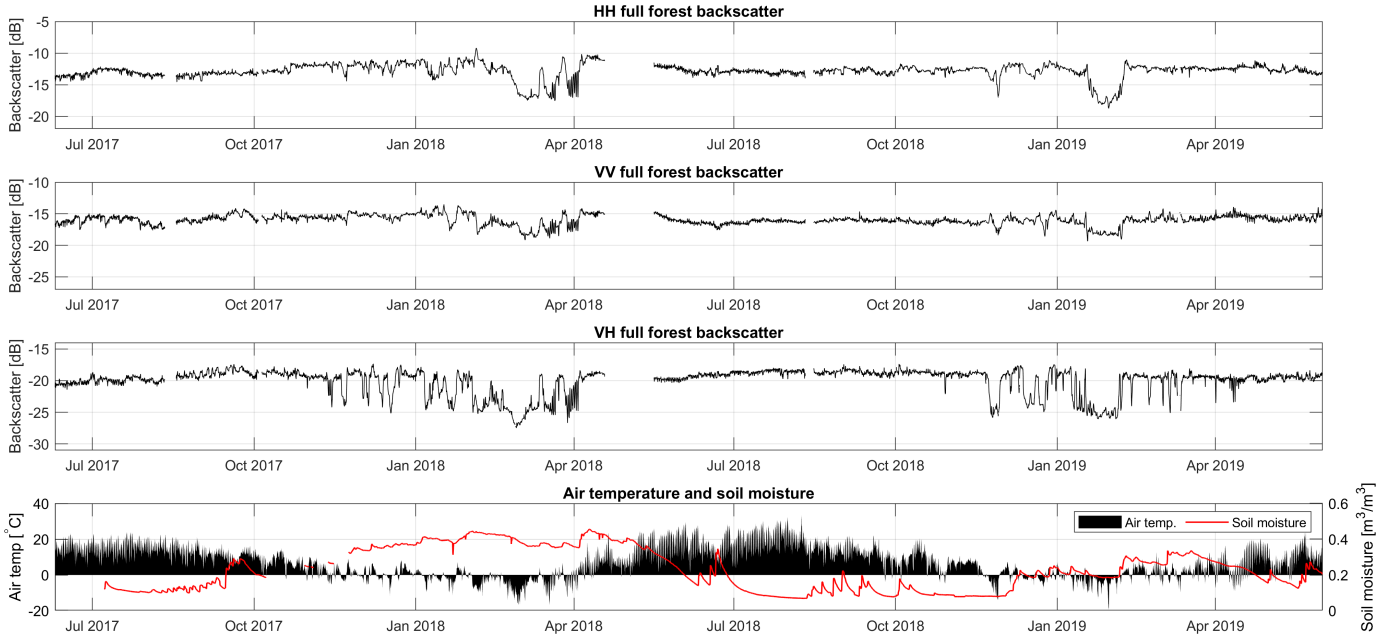

Fig. 7. Time series of the temporally-smoothed full forest backscatter, air temperature and soil moisture.

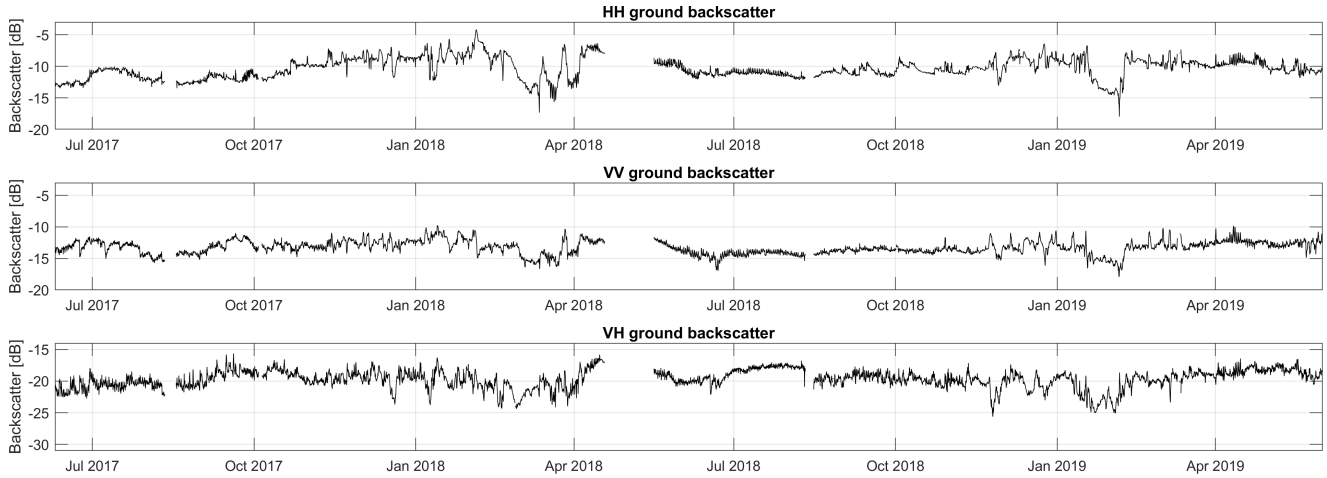

Fig. 8. Time series of the temporally-smoothed ground-level backscatter.

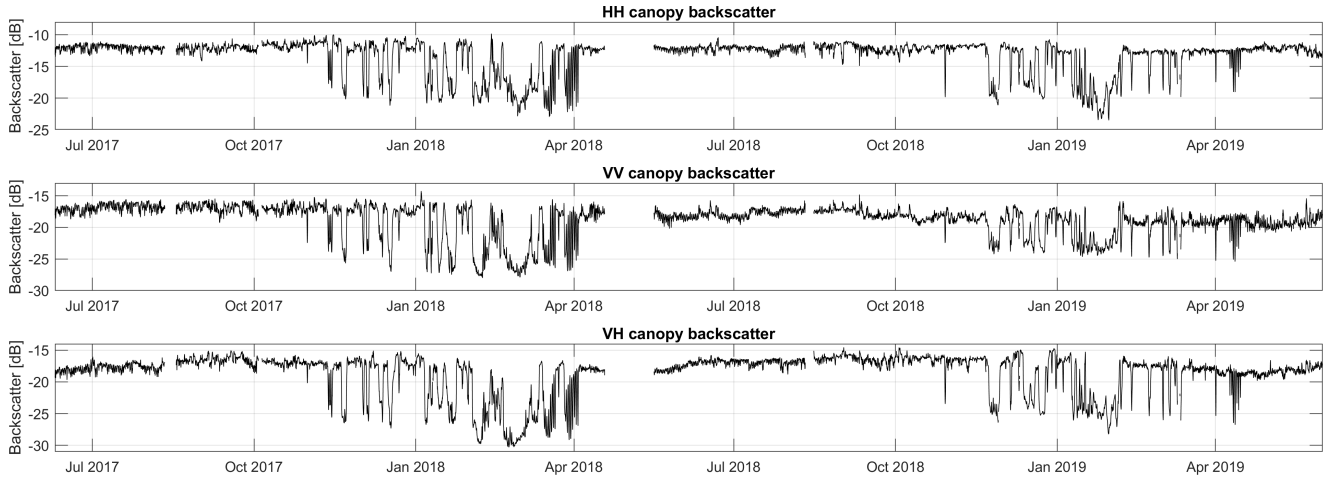

Fig. 9. Time series of the temporally-smoothed canopy backscatter.

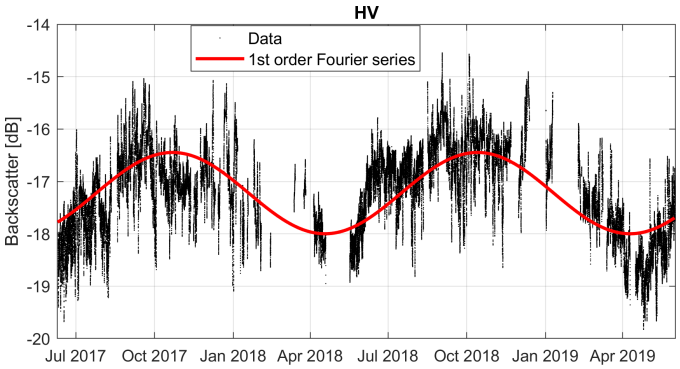

Fig. 10. VH canopy backscatter and a 1st order Fourier series fit showing a seasonal component. Frozen conditions were manually removed from the backscatter data.

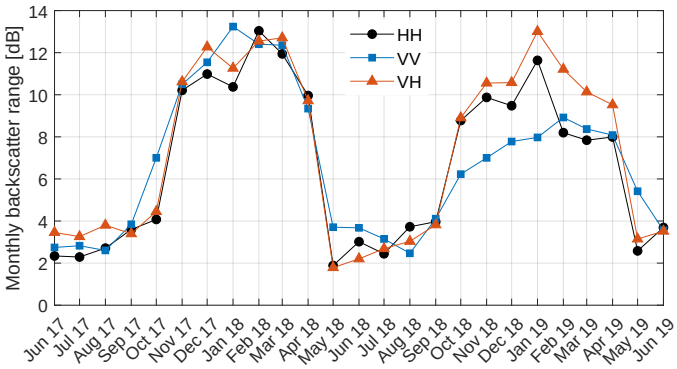

Fig. 11. Monthly range of the canopy backscatter. The winter periods show the largest range of canopy intensities due to freeze-thaw cycles and do not vary significantly between polarizations, except for VV in the winter of 2018-2019.

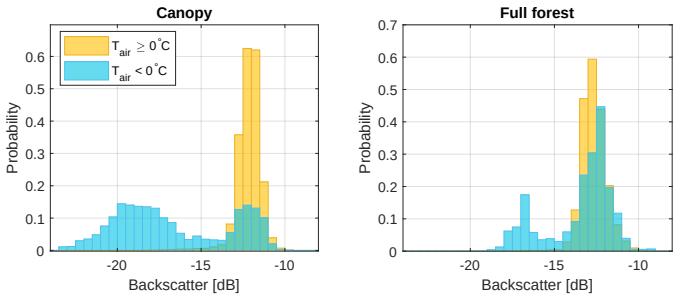

Fig. 12. Histograms showing the HH backscatter distributions for temperatures above and below 0°C for the entire observation period. Other polarizations show similar distribution differences.

HH and VV. Short-term variations (2 to 3 dB), which are not visible in the full-forest backscatter, are amplified by the decibel scale since the canopy backscatter is weaker than the full-forest backscatter. VH canopy backscatter does not show a significant improvement in stability compared to the full-forest backscatter in Fig. 7 since the ground contribution is insignificant. The similarity in canopy-level backscatter dynamics between polarizations indicates that the underlying scattering mechanism is independent of polarization. This mechanism is volume scattering, in which the scattered electric field is the coherent sum of contributions of many, randomly orientated scattering elements within a resolution cell. This makes the canopy-level backscatter independent of soil moisture content. The only significant difference seen between polarizations is that the VH canopy backscatter exhibits a seasonal component with a peak-to-peak amplitude of approximately (2 dB) during non-frozen conditions. This is shown in Fig 10. The cause of this seasonal backscatter cycle, which is only visible for VH, is not clear from the available data. Possible causes could be seasonal moisture variations, tree ring formation or reproduction cycles.

B. *Effects of freeze-thaw cycles*

Freeze-thaw cycles cause the largest variations in P-band canopy backscatter. This is most clearly seen in the monthly peak-to-peak backscatter range shown in Fig. 11. The canopy backscatter range has a seasonal cycle, reaching up to 13 dB during the winter. There is no significant difference between polarizations, except that the canopy backscatter range for VV is lower than that of other polarizations during the early winter of 2018-2019. This is likely due to the warmer temperatures of the 2018-2019 winter.

The canopy backscatter is significantly lower during freezing temperatures, as is shown by the HH canopy backscatter distributions in Fig. 12. This is because part of the free water in the trees turns into ice, which has a significantly lower permittivity compared to liquid water [39], [40], resulting in weaker reflections of electromagnetic waves. The distribution of canopy backscatter during freezing temperatures is bimodal, showing that the vegetation does not freeze at the exact onset of sub-zero air temperatures. This may be due to a difference in air and tree temperatures or because free water in vegetation may exist in a supercooled state before ice nucleation occurs [28], [41], [42]. Canopy and full forest backscatter were comparably stable during non-frozen conditions, with a standard deviation of 0.7 to 1 dB.

A sample of the HH backscatter time series during the winter is shown in Fig. 13 for closer inspection. The canopy backscatter drops significantly (up to 10 dB) when the air temperature around the canopy drops from positive to negative temperatures. Moisture in the canopy freezes rapidly, making the canopy more transparent to a P-band radar. This is true for all polarizations. The reduced canopy attenuation during freezing temperatures results in an increase in ground-level backscatter at the onset of negative temperatures. Canopy and ground-level backscatter for HH and VV counteract one another during freeze-thaw cycles. As a result, the full forest backscatter, which is the sum of the canopy and ground-level reflections, shows little freeze-thaw variation for much of the winter (see Fig. 7). However, during sustained negative air temperatures, the ground and lower tree trunks gradually freeze, reducing the double-bounce scattering and lowering the ground-level backscatter. This leads to large drops in full-forest backscatter during the winter. Freeze-thaw cycles for HH and VV have a significant impact on tomographic P-band SAR, but the full-forest backscatter is only affected during sustained negative air temperatures. For VH, canopy scattering dominates the full-forest backscatter, causing large variations

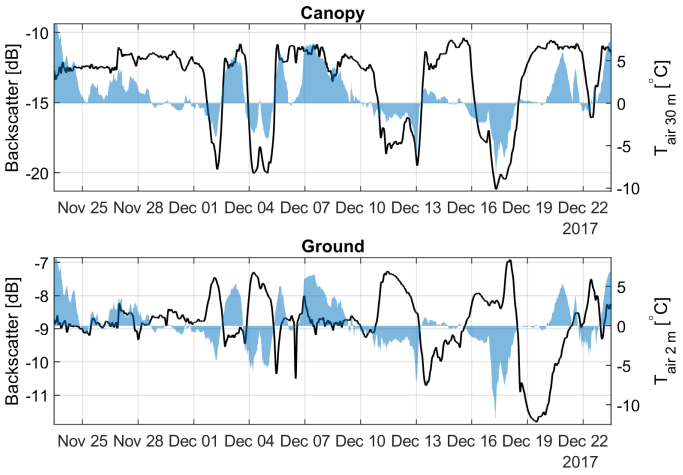

Fig. 13. Canopy and ground-level tomographic backscatter for HH-polarization during freeze-thaw cycles. Canopy backscatter drops significantly during freezing temperatures. Ground-level backscatter is stronger in freezing temperatures because the canopy attenuation is lower. For sustained freezing temperatures, the ground backscatter eventually decreases as it freezes from the top down.

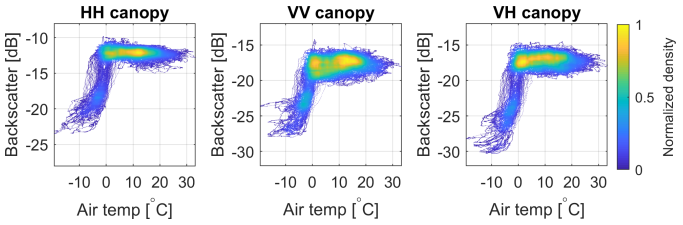

Fig. 14. Scatterplots of the canopy backscatter vs. air temperature. A strong correlation between negative air temperatures and canopy backscatter exists due to varying ice fractions in the trees.

in both canopy and full-forest backscatter during freeze-thaw cycles.

A strong positive correlation is observed between canopy backscatter and air temperature during freezing conditions in the scatterplots in Fig. 14. The dielectric properties of ice have a negligible temperature dependence below 0°C [43], [44], and do not cause the observed backscatter variations. Instead, these observations are due to a varying fraction of free water in the trees which turns into ice [45]. The ice fraction of wood, and thus its permittivity, is strongly temperature dependent for sub-zero temperatures [46].

The freeze-thaw dynamics of the ground-level backscatter are more complicated because canopy freezing, stem freezing and ground freezing do not necessarily occur at the same time. Spatio-temporal ice formation mechanisms in trees are not well understood and the role of ground freezing in the observed freeze-thaw dynamics is not clear from this study. Our results agree with previous studies that the canopy freezes first [28], [47], after which the lower trunk gradually freezes over the timescale of hours. Ground backscatter exhibits polarization-dependent hysteresis during freeze-thaw cycles [48]. However, the freezing dynamics in the trunks and soil cannot be separated in tomographic imaging, complicating the modelling and interpretation of ground-level freeze-thaw dynamics.

C. Effects of snow cover and melting snow

The upper canopy backscatter does not appear to be affected by snow. Surveillance camera footage showed that snow collecting on branches caused the branches to sag. This change in geometry had no observable effect on the upper-canopy backscatter since the branches were mostly transparent to P-band radar during sub-zero air temperatures. The upper canopy backscatter changes were instead more clearly correlated with temperature variations, which through the canopy attenuation affects the ground-level backscatter. Snow that collected on the ground (10 cm) also had no distinguishable effect on ground-level backscatter.

The effect of melting snow is difficult to examine since it is usually accompanied by an air temperature change from negative to positive degrees Celsius, which dominates backscatter variations. Rain is often the cause of snow melting on the ground, which causes a clear increase in ground-level backscatter in channels where the ground plays a significant role (HH and VV). HH and VV backscatter were closely correlated with soil moisture content when the snow was melting. Snow on the ground melting in the absence of rain did not show any significant change in ground-level backscatter.

These results suggest that snow has no significant effect on P-band radar observations of the studied forest site. However, this site did not experience long-term, heavy snowfall during the observation period, leaving these results inconclusive.

D. Diurnal variations

Backscatter variations on diurnal timescales were observed during the summers. Fig. 15 shows an example of diurnal backscatter cycles for HH during the hot summer of 2018, along with the VPD. The VPD reaches high values during mid-day, which is an indication of a high rate of transpiration. During these high rates of transpiration, the canopy backscatter decreases, increasing again in the late afternoon. This is likely due to a decrease of tree water content in the upper canopy, which both decreases the amount of backscattered power and decreases the canopy attenuation. When the VPD is very high, trees risk undergoing permanent damage whereby the water columns in xylem vessels break apart due to low pressures, becoming air-filled (cavitation) [49]. To regulate this pressure, trees may close their stomata in the middle of the day, limiting transpiration and halting the decrease in tree water content [50]. The effect of this midday stomatal closure is likely seen every day in Fig. 15 as a bump in canopy backscatter around noon. The bump in ground-level backscatter also coincided with the midday stomatal closure. A possible reason for this is because the sap flow rate in the stem is high at the onset of stomatal closure, temporarily causing an increase in stem water content, similar to a hydraulic shock. A decrease in canopy attenuation during the day will also contribute to the ground-level backscatter diurnal cycles. Therefore, spatio-temporal water transport in the trees appear to play a role in the observed diurnal backscatter variations. Diurnal cycles can be seen in all polarizations as is shown in Fig. 16. These average diurnal patterns were extracted over the period from 17 May to 9 August 2018. The patterns for HH and VV are very similar and

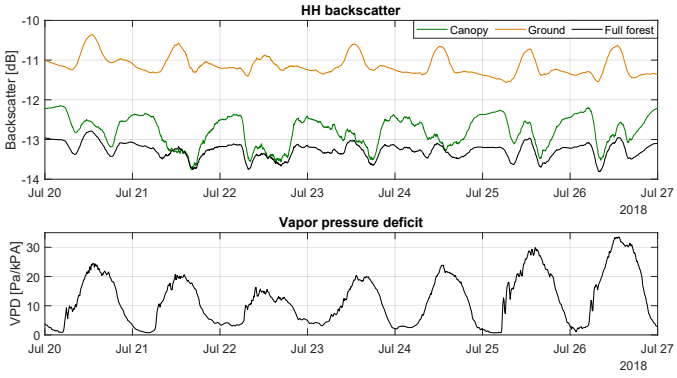

Fig. 15. Diurnal cycles in HH backscatter during the summer of 2018. A high VPD indicates high rates of transpiration, making the canopy lose moisture. This reduces the backscattered power from the canopy and reduces canopy attenuation, increasing double-bounce scattering seen at the ground level. The tick mark corresponds to midnight each day.

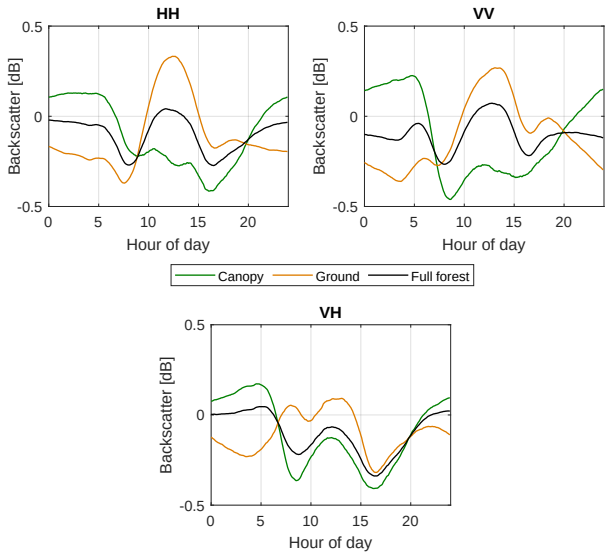

Fig. 16. Mean diurnal cycles for the summer period of 17 May 2018 to 9 August 2018. All polarizations show a decrease in canopy backscatter and increase in ground-level backscatter around noon when the transpiration rate is highest.

the midday stomatal closure is most clearly seen in VH canopy backscatter. It may appear that the variance in backscatter, as measured by polar-orbiting SARs, can be minimized by choosing an overpass time of day when the trees are less likely to be affected by transpiration (e.g. midnight to dusk). Such a choice does unfortunately not decrease the variance since diurnal cycles are only visible during the warmest period of the year (May to August) and are superimposed onto variations over longer timescales that have as much variance as the diurnal cycles themselves.

Diurnal cycles, as are shown in Figs. 15 and 16, are most clearly visible during periods with high evaporative demand. A high evaporative demand is caused by warm air temperatures, low relative humidity, unobstructed sunlight and moderate-to-high wind speeds. Diurnal backscatter variations have also been observed in a tropical forest during the dry season [2]. In dry conditions, the rate of evaporation exceeds the rate of water uptake by the roots in the morning, resulting in a depletion of the tree's internal water reserves [24], [25], [51]. Depletable water reserves are believed to reside in the bark and sapwood. It is this decrease in water content which results in the observed decrease in canopy backscatter and attenuation. The water reserves are replenished later in the day and during the night through ground water uptake when the evaporative demand decreases, increasing the canopy backscatter again. The onset of transpiration in the morning does not always result in a decrease in canopy backscatter. This is the case when the evaporative demand is likely not high enough (e.g. too little sunlight during the autumn) to cause the depletion of the tree's water reserves. The trees are thus capable of transpiring without decreasing their water content, which has no visible effect on the mean radar backscatter. The tree water reserves only serve as a buffer between root water uptake and release through transpiration [24]. These observations indicate that P-band radar measurements of forests are sensitive to the diurnal transpiration cycles in boreal forests and that, under certain environmental conditions, biophysiological variables such as transpiration rate and tree water content may be sensed using P-band radar.

E. Effects of rain

During rainfall, much of the rain is intercepted by the forest canopy. This increase in water content in the canopy can be expected to have an effect on the observed backscatter. The effect of rain during the summer of 2018 is shown in Fig. 17. During the three heavy rainfall periods (A, B and C in Fig. 17), the canopy backscatter increased for all polarizations, most significantly for HH and VV (1 to 2 dB). This indicates that the intercepted rainfall increases canopy backscatter due to an increase in canopy water content. One can therefore expect an increase in canopy attenuation, leading to a decrease in ground-level backscatter during heavy rain. Such a drop in ground-level backscatter was only seen for VV and VH in Fig. 17, whereas the ground-level backscatter for HH increased during rain. The rainfall events are accompanied by a large increase in soil moisture at the ground surface. Such an increase in soil moisture should affect both HH and VV ground-level backscatter with approximately the same magnitudes since the soil Fresnel reflection coefficients for both horizontally- and vertically-polarized waves at oblique incidence increase by approximately the same magnitudes with an increase in soil moisture [35]. The difference between the behavior of HH and VV ground-level backscatter during heavy rainfall must therefore be due to different canopy attenuation mechanisms, whereby heavy rainfall increases the canopy attenuation for VV more than for HH.

The light rainfall events (D and E in Fig. 17) did not have any significant effect on the observed backscatter. Since heavy rainfall such as events A, B and C in Fig. 17 are rare in this region, rain rarely has any noticeable effect on tomographic image backscatter at P-band. Events A, B and C in Fig. 17 should therefore be considered as extreme cases. These observations agree with studies that have shown that while rainfall can lead to an increase in the permittivity of trees, some rainfall events have no effect [52], [53].

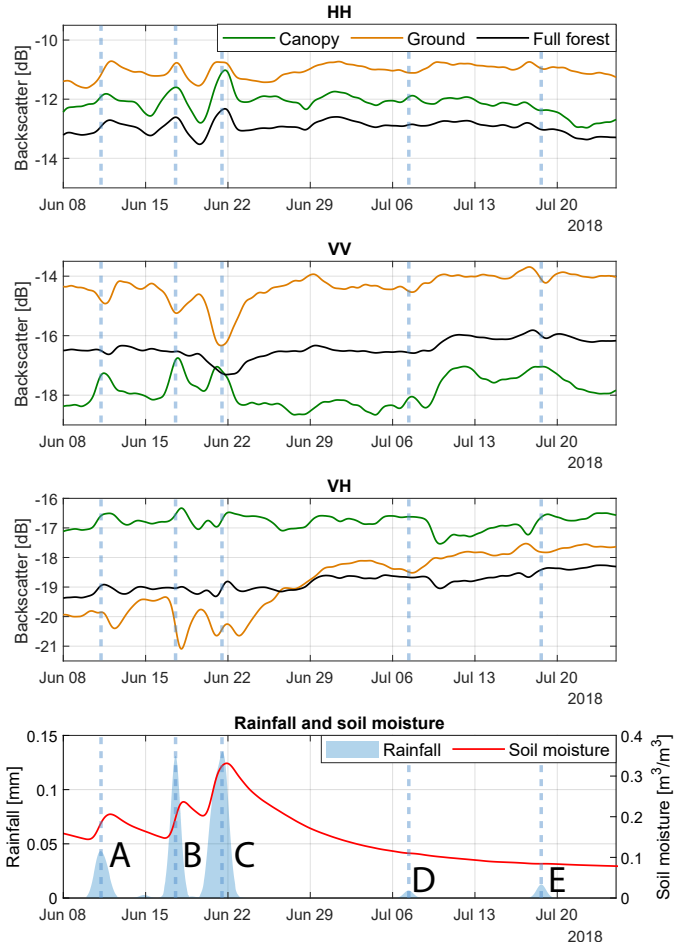

Fig. 17. Canopy, ground-level and full forest backscatter time series along with the rainfall. The dashed blue lines and labels A to E mark the times at which rainfall occurs. The time series were smoothed to remove diurnal variations. Heavy rain has a clear effect on canopy and ground-level backscatter whereas light rain does not have any significant effect.

F. Effects of wind

Wind causes geometric changes in the observed scene as trees sway in the wind. These geometric changes cause fluctuations in the observed backscatter. Fig. 18 shows the observed canopy backscatter with and without temporal averaging (smoothing) as well as the average wind speed for a period during the 2017 summer. During periods with strong winds (>5 m/s), large backscatter fluctuations over timescales of hours can be seen. This is temporal speckle, or Rayleigh fading, which occurs when the scattered fields from scattering elements in the forest interfere constructively and destructively over time. The standard deviation of the short-term canopy backscatter fluctuations caused by wind increases with wind speed as is shown in Fig. 19. This is true for all polarizations. During summer nights and mornings, there was little wind, making the backscatter very stable over timescales of hours.

The temporally-averaged backscatter time series in Fig. 18 also show that strong winds coincide with a drop in average canopy backscatter. A similar drop in full forest backscatter was previously observed in non-tomographic measurements [4], which was attributed to decreased double-bounce scattering as the trees bend in the wind. The motivation for this interpretation was that the drop in backscatter was not seen for VH polarization, which is less sensitive to double-bounce scattering. However, the tomographic data shows that a drop in the canopy backscatter during high wind speeds, as in Fig. 18, occurs for all polarizations. Since the relationship between canopy backscatter and wind speed is not one-to-one, they are best compared with their rates of change with time, as is shown in Fig. 20. An increase in wind speed causes a decrease in the canopy backscatter of HH, VV and VH, and an increase in the ground backscatter of only VH. This increase in VH ground backscatter is likely due to increased double-bounce scattering between the bending stems and the ground [54], counteracting the decrease canopy backscatter during windy conditions. This explains why the effect was not seen in [4] for cross-polarized full forest backscatter. These results show that a change in double-bounce scattering is not the sole underlying mechanism behind the decrease in backscatter during strong winds. A more likely cause of the observed drop in canopy backscatter is the depletion of water in the canopy during strong winds. When trees transpire, the air at the leaf surface becomes saturated with water vapor leaving the stomata, decreasing the evaporative demand and inhibiting transpiration [50], [55]. Wind replaces the saturated air with dry air, increasing the VPD at the stomata and increasing the rate of transpiration [56], [57]. The high rate of transpiration during strong winds decreases the tree water content, causing a decrease in canopy backscatter.

The mechanism by which wind causes a decrease in mean canopy backscatter is the same mechanism causing diurnal cycles. This theory is supported by the observation that strong winds during cold conditions do not cause a decrease in mean canopy backscatter. Strong winds with little solar radiation will cool the stomata, preventing transpiration [56]. Transpiration will also be low if the relative humidity is high. Under cold or humid conditions, depletion of the tree's internal water reserves is not necessary to sustain the transpiration rate demanded by the atmosphere.

V. Discussion

The largest backscatter variations observed were caused by freezing temperatures. The large drops in canopy (as well as full forest) backscatter during frozen conditions may result in large errors in forest parameter estimates and forest disturbance detections using P-band SAR data. Correcting for this drop is not simple since the permittivity of wood is strongly dependent on temperature during frozen conditions. The best approach would be to discard SAR observations acquired during frozen conditions, but this requires frozen conditions to be detected. Such a detection is complicated by the observation that the drop in backscatter does not occur until a few degrees below 0°C, and thawing may not occur until several degrees above 0°C. Therefore, air temperature cannot be used as a reliable proxy. Another complication is that while the canopy may be frozen, the effect might not be seen in the full forest HH and VV backscatter as observed by a single SAR overpass. However, this was not the case for

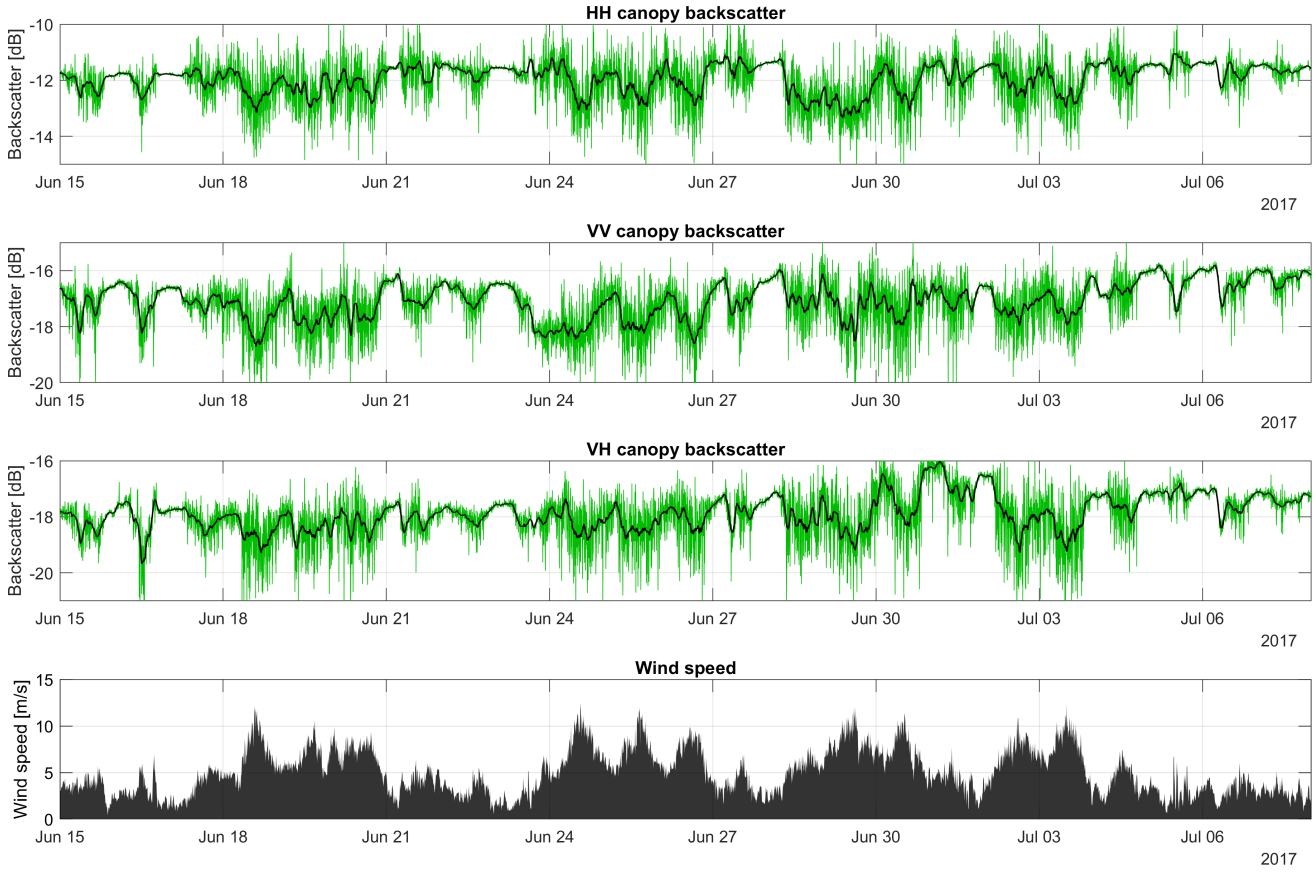

Fig. 18. Time series of the canopy backscatter and wind speed during the 2017 summer. The green curve is the observed backscatter and the black curve is the observed backscatter after smoothing. Strong winds cause both short-term fluctuations in backscatter and a drop in mean backscatter.

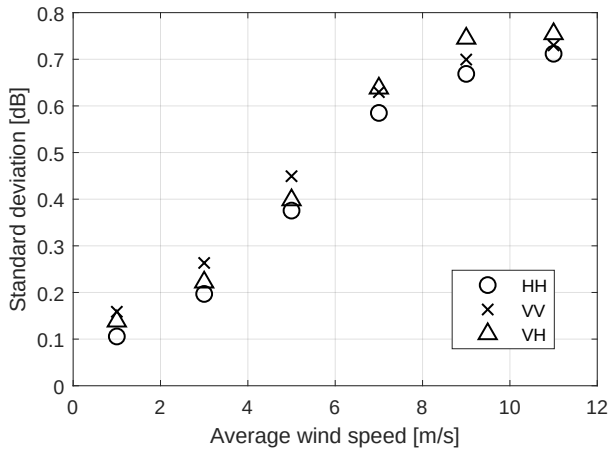

Fig. 19. Short-term standard deviations of the canopy backscatter (not temporally smoothed) as a function of wind speed for the entire dataset. Backscatter fluctuations increase in standard deviation when the wind speed increases.

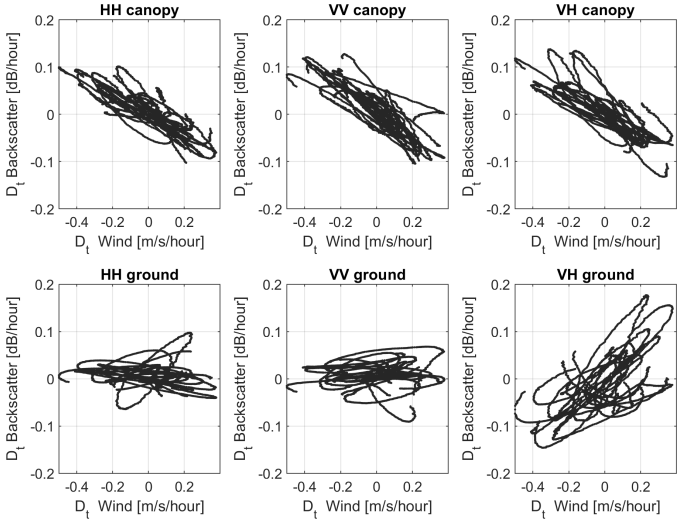

Fig. 20. Derivative of the mean backscatter vs. the derivative of wind speed. The canopy backscatter decreases when wind speed increases. The opposite behavior is seen for VH ground-level backscatter.

cross-polarized observations. Therefore, the best possibility for detecting frozen conditions from backscatter data is to detect changes (>2 dB) in cross-polarized backscatter between SAR overpasses. Large drops in cross-polarized backscatter, which do not appear in co-polarized backscatter, are likely due to frozen trees during the time of overpass and not deforestation. However, during sustained frozen conditions, the co-polarised channels will also show a drop in backscatter. Therefore, this approach is questionable for other forest densities and climates. The possibility of using phase shifts for detecting freezing conditions should be investigated in the future.

HH and VV full forest backscatter were influenced by

large variations (3 to 5 dB) in ground-level backscatter due to soil moisture changes. However, the full forest variations during non-frozen conditions were no larger than those of VH since the much more stable canopy backscatter contributed significantly to the full forest backscatter for all polarizations in this dense forest. In forests of lower density, and thus less canopy backscatter and attenuation, soil moisture variations can be expected to play a larger role in full forest HH and VV backscatter. Canopy backscatter was very stable over long timescales. Therefore. canopy backscatter will be accurately rendered by repeat-pass SAR tomography and ground-notching interferometry, assuming high temporal coherence.

P-band backscatter observations were, for the first time, explained using tree water transport dynamics. The diurnal variations in backscatter observed in this study were small enough ($<$1 dB) to not have a significant impact on forest parameter estimates using SAR data. The long revisit times of polar-orbiting, sun-synchronous SARs makes them unable to capture the diurnal dynamics of forest backscatter. Other SAR mission designs utilizing multiple spaceborne SAR platforms, high-altitude platform systems (HAPS) or geostationary orbits may be capable of capturing diurnal forest backscatter patterns. Information about the water transport in forests is important for ecophysiology, soil water dynamics and the management of watersheds. Tower-based radars can be used as a new tool for characterizing and monitoring tree water content signatures over spatial scales of forest stands to ecosystems. Changes in tree water content can be used to constrain canopy conductance, which is a key variable in soil-vegetation-atmosphere transport models, ecosystem productivity models and global climate models [58]. Although only a single tree species was observed in this study, trees of different species have very similar diurnal characteristics of water transport [59], and can be expected to show similar backscatter signatures.

The canopy backscatter diurnal cycles resemble the temporal signatures of stem radii as measured by dendrometers. These cycles can be described as a constant value that dips during the day. Diurnal variations in stem permittivity are more sinusoidal than those measured by dendrometers [40], [52]. However, radar backscatter is more closely related to permittivity than stem radius. This discrepancy may partially be explained by the nonlinear relationship between permittivity and backscatter [18]. The relationship between canopy backscatter and the permittivity measured at a single point in a stem may also be more complicated than what is currently accepted. To the authors' knowledge, no experimental work has been carried out in which both backscatter and permittivity were measured over diurnal timescales. Time series of the *in-situ* permittivity of upper canopy structures has also not been acquired yet.

Short-term fluctuations in backscatter due to wind are not expected to affect P-band SAR observations. The temporal statistics of forest backscatter fluctuations has been observed to be similar to the spatial statistics [60]. Spatial multilooking will average out these fluctuations. However, repeat-pass techniques such as interferometry and tomography will be affected by these fluctuations in the form of temporal decorrelation. Drops in backscatter caused by strong winds will only affect 6 pm overpasses during warm days as the decrease in water content was observed to persist into the late afternoon.

Finally, this study leaves many unanswered questions. The origin of canopy-level backscatter is not clear for the different polarizations. A decrease in canopy backscatter did not always appear to coincide with a reduction of canopy attenuation. Many backscatter variations observed in this study could not be explained using the available weather and soil moisture data. Separation of backscatter contributions from different regions in the forest is difficult even with tomographic radar. Changes in ground-level backscatter, which has a significant influence on HH and VV full forest backscatter, can be caused by canopy attenuation, stem water content, or soil moisture content variations. These effects could not be separated in this study, complicating the interpretation of the effects of freeze-thaw cycles, strong winds and rain. Future work will include the analysis of backscatter data along with dendrometer, sap flow, and soil moisture profile data. Measurements of the *in-situ* permittivity will also be made since there is a possibility that the stem water content and permittivity can be affected by chemical changes [52], [61]. Measurements of the complex permittivity will also clarify the relationship between backscatter and attenuation in forest canopies. Finally, a similar analysis for phase shifts and for observations at other frequency bands (e.g. L-band and C-band) will be done, providing deeper insight into the electromagnetic scattering mechanisms and spatio-temporal backscatter variations.

VI. Conclusions

In this study, a mature stand of Norway spruce was monitored by a multi-polarimetric, tomographic tower-based radar over a two-year period. Time series of the forest backscatter, ground-level backscatter and upper-canopy backscatter were extracted from tomographic images and analyzed in relation to meteorological variables. Temporal variations in backscatter due to seasonal changes, freezing temperatures, diurnal variations, rain and wind were characterized and quantified. Observations were related to the underlying electromagnetic scattering mechanisms, relative permittivity and ecophysiology. Forest backscatter was observed to be sensitive to changes in the state of water in trees. Depleting water reserves in trees due to high rates of transpiration during hot, windy days were clearly visible in forest backscatter. Many variations in the observed backscatter could not be explained using ancillary data. These results give insight into the effects of seasonal and weather changes on forest parameter estimates using SAR data. The results also open up new opportunities for monitoring tree water status using P-band imaging radars.

Acknowledgment

The authors would like to thank the Swedish Defence Research Agency (FOI) for providing and installing the trihedral corner reflectors at the experimental site and the Swedish University of Agricultural Sciences (SLU) for providing the terrestrial lidar point cloud of the forest site.

REFERENCES

[1] C. Albinet, P. Borderies, N. Floury, and E. Pottier, "Measure of temporal variation of P-band radar cross section and temporal coherence of a temperate tree," *IEEE Transactions on Geoscience and Remote Sensing*, vol. 54, no. 11, pp. 6255–6264, 2016.

[2] A. Hamadi, C. Albinet, P. Borderies, T. Koleck, L. Villard, D. Ho Tong Minh, and T. Le Toan, "Temporal survey of polarimetric P-band scattering of tropical forests," *IEEE Transactions on Geoscience and Remote Sensing*, vol. 52, no. 8, 2014.

[3] J. T. Pulliainen, L. Kurvonen, and M. T. Hallikainen, "Multitemporal behavior of L- and C-band SAR observations of boreal forests," *IEEE Transactions on Geoscience and Remote Sensing*, vol. 37, no. 2 II, pp. 927–937, 1999.

[4] A. R. Monteith and L. M. H. Ulander, "Temporal survey of P- and L-band polarimetric backscatter in boreal forest," *IEEE Journal of Selected Topics in Applied Earth Observations and Remote Sensing*, vol. 11, no. 10, pp. 3564–3577, 2018.

[5] ESA (2012), *Report for Mission Selection: BIOMASS*. ESA SP-1324/1 (3 volume series), European Space Agency, Noordwijk, The Netherlands.

[6] S. Quegan, T. Le Toan, J. Chave, J. Dall, J.-F. Exbrayat, D. H. T. Minh, M. Lomas, M. M. D'Alessandro, P. Paillou, K. Papathanassiou, F. Rocca, S. Saatchi, K. Scipal, H. Shugart, T. Smallman, M. J. Soja, S. Tebaldini, L. M. H. Ulander, L. Villard, and M. Williams, "The European Space Agency BIOMASS mission: Measuring forest above-ground biomass from space," *Remote Sensing of Environment*, vol. 227, pp. 44–60, 2019.

[7] T. Le Toan, A. Beaudoin, J. Riom, and D. Guyon, "Relating forest biomass to SAR data," *IEEE Transactions on Geoscience and Remote Sensing*, vol. 30, no. 2, pp. 403–411, 1992.

[8] M. C. Dobson, F. T. Ulaby, T. Le Toan, A. Beaudoin, E. S. Kasischke, and N. Christensen, "Dependence of radar backscatter on coniferous forest biomass," *IEEE Transactions on Geoscience and Remote Sensing*, vol. 30, no. 2, pp. 412–415, 1992.

[9] H. Israelsson, J. Askne, and R. Sylvander, "Potential of SAR for forest bole volume estimation," *International Journal of Remote Sensing*, vol. 15, no. 14, pp. 2809–2826, 1994.

[10] S. H. Alemohammad, T. Jagdhuber, M. Moghaddam, and D. Entekhabi, "Soil and vegetation scattering contributions in L-band and P-band polarimetric SAR observations," *IEEE Transactions on Geoscience and Remote Sensing*, vol. 57, no. 11, pp. 8417–8429, 2019.

[11] F. Banda, D. Giudici, T. Le Toan, M. Mariotti dAlessandro, K. Papathanassiou, S. Quegan, G. Riembauer, K. Scipal, M. J. Soja, S. Tebaldini, L. M. H. Ulander, and L. Villard, "The BIOMASS Level 2 prototype processor: Design and experimental results of above-ground biomass estimation," *Remote Sensing*, vol. 12, no. 6, 2020.

[12] M. J. Soja, G. Sandberg, and L. M. H. Ulander, "Regression-based retrieval of boreal forest biomass in sloping terrain using P-band SAR backscatter intensity data," *IEEE Transactions on Geoscience and Remote Sensing*, vol. 51, no. 5, pp. 2646–2665, 2013.

[13] D. H. T. Minh, T. Le Toan, F. Rocca, S. Tebaldini, L. Villard, M. Rjou-Mchain, O. L. Phillips, T. R. Feldpausch, P. Dubois-Fernandez, K. Scipal, and J. Chave, "SAR tomography for the retrieval of forest biomass and height: Cross-validation at two tropical forest sites in french guiana," *Remote Sensing of Environment*, vol. 175, pp. 138–147, 2016.

[14] S. Tebaldini and F. Rocca, "Multibaseline polarimetric SAR tomography of a boreal forest at P- and L-bands," *IEEE Transactions on Geoscience and Remote Sensing*, vol. 50, no. 1, pp. 232–246, 2012.

[15] M. J. Soja, M. M. D'Alessandro, S. Quegan, S. Tebaldini, and L. M. H. Ulander, "Model-based estimation of tropical forest biomass from notch-filtered P-band Sar backscatter," *IGARSS 2018 - 2018 IEEE International Geoscience and Remote Sensing Symposium*, pp. 8617–8620, July 2018.

[16] F. T. Ulaby, "Radar response to vegetation," *IEEE Transactions on Antennas and Propagation*, vol. 23, no. 1, pp. 36–45, 1975.

[17] E. Puttonen, C. Briese, G. Mandlburger, M. Wieser, M. Pfennigbauer, A. Zlinszky, and N. Pfeifer, "Quantification of overnight movement of birch (betula pendula) branches and foliage with short interval terrestrial laser scanning," *Frontiers in Plant Science*, vol. 7, no. FEB2016, 2016.

[18] M. Moghaddam, S. Durden, and H. Zebker, "Radar measurement of forested areas during OTTER," *Remote Sensing of Environment*, vol. 47, no. 2, pp. 154–166, 1994.

[19] D. Solimini, *Understanding Earth Observation: The Electromagnetic Foundation of Remote Sensing*. Springer International Publishing Switzerland, 2016.

[20] M. T. Hallikainen, F. T. Ulaby, M. C. Dobson, M. A. El-Rayes, and L.-K. Wu, "Microwave dielectric behavior of wet soil-part I: Empirical models and experimental observations," *IEEE Transactions on Geoscience and Remote Sensing*, vol. GE-23, no. 1, pp. 25–34, 1985.

[21] N. R. Peplinski, F. T. Ulaby, and M. C. Dobson, "Dielectric Properties of Soils in the 0.3-1.3-GHz Range," *IEEE Transactions on Geoscience and Remote Sensing*, vol. 33, no. 3, pp. 803–807, 1995.

[22] M. Moghaddam, S. Saatchi, and R. H. Cuenca, "Estimating subcanopy soil moisture with radar," *Journal of Geophysical Research Atmospheres*, vol. 105, no. D11, pp. 14 899–14 911, 2000.

[23] H. H. Dixon and J. Joly, "On the ascent of sap," *Philosohpical Transactions of the Royal Society B*, vol. 186, pp. 563–576, 1895.

[24] R. Zweifel, H. Item, and R. Häsler, "Link between diurnal stem radius changes and tree water relations," *Tree Physiology*, vol. 21, no. 12-13, pp. 869–877, 2001.

[25] S. Pfautsch, T. Hölttä, and M. Mencuccini, "Hydraulic functioning of tree stems - fusing ray anatomy, radial transfer and capacitance," *Tree Physiology*, vol. 35, no. 7, pp. 706–722, 2015.

[26] P. G. Jarvis, "The interpretation of the variations in leaf water potential and stomatal conductance found in canopies in the field," *Philosophical Transactions of the Royal Society of London. B, Biological Sciences*, vol. 273, no. 927, pp. 593–610, 1976.

[27] T. Kumagai, *Forest Hydrology and Biogeochemistry: Synthesis of Past Research and Future Directions*. Springer, Dordrecht, 2011, ch. Transpiration in Forest Ecosystems.

[28] G. Charrier, M. Nolf, G. Leitinger, K. Charra-Vaskou, A. Losso, U. Tappeiner, T. Amglio, and S. Mayr, "Monitoring of freezing dynamics in trees: A simple phase shift causes complexity," *Plant Physiology*, vol. 173, no. 4, pp. 2196–2207, 2017.

[29] L. M. H. Ulander, A. R. Monteith, M. J. Soja, and L. E. B. Eriksson, "Multiport vector network analyzer radar for tomographic forest scattering measurements," *IEEE Geoscience and Remote Sensing Letters*, vol. 15, no. 12, pp. 1897–1901, 2018.

[30] H. T. M. Dinh, S. Tebaldini, F. Rocca, T. Koleck, P. Borderies, C. Albinet, L. Villard, A. Hamadi, and T. Le Toan, "Ground-based array for tomographic imaging of the tropical forest in P-band," *IEEE Transactions on Geoscience and Remote Sensing*, vol. 51, no. 8, pp. 4460–4472, 2013.

[31] A. R. Monteith, L. M. H. Ulander, and S. Tebaldini, "Calibration of a ground-based array radar for tomographic imaging of natural media," *Remote Sensing*, vol. 11, no. 24, pp. 1–22, 2019.

[32] J. A. Goff, "Low-pressure properties of water-from 160 to 212°F." *Transactions of the American Society of Heating and Ventilating Engineers*, vol. 52, pp. 95–121, 1946.

[33] V. Cazcarra-Bes, M. Pardini, M. Tello, and K. P. Papathanassiou, "Comparison of tomographic SAR reflectivity reconstruction algorithms for forest applications at L-band," *IEEE Transactions on Geoscience and Remote Sensing*, vol. 58, no. 1, pp. 147–164, 2020.

[34] M. Moghaddam and S. Saatchi, "Analysis of scattering mechanisms in SAR imagery over boreal forest: Results from BOREAS '93," *IEEE Transactions on Geoscience and Remote Sensing*, vol. 33, no. 5, pp. 1290–1296, 1995.

[35] F. T. Ulaby, D. G. Long, W. J. Blackwell, C. Elachi, A. K. Fung, C. Ruf, K. Sarabandi, H. A. Zebker, and J. Van Zyl, *Microwave radar and radiometric remote sensing*. University of Michigan Press Ann Arbor, 2014.

[36] J. Lee and E. Pottier, *Polarimetric Radar Imaging*. Taylor & Francis Group, Boca Raton, USA, 2009.

[37] R. W. Schafer, "What is a Savitzky-Golay Filter? [lecture notes]," *IEEE Signal Processing Magazine*, vol. 28, no. 4, pp. 111–117, 2011.

[38] A. Khoshrou, A. B. Dorsman, and E. J. Pauwels, "SVD-based visualisation and approximation for time series data in smart energy systems," *2017 IEEE PES Innovative Smart Grid Technologies Conference Europe, ISGT-Europe 2017 - Proceedings*, vol. 2018-January, pp. 1–6, 2017.

[39] J. Way, J. Paris, E. Kasischke, C. Slaughter, L. Viereck, N. Christensen, M. C. Dobson, F. T. Ulaby, J. Richards, A. Milne, A. Sieber, F. J. Ahern, D. Simonett, R. Hoffer, M. Imhoff, and J. Weber, "The effect of changing environmental conditions on microwave signatures of forest ecosystems: Preliminary results of the March 1988 Alaskan aircraft SAR experiment," *International Journal of Remote Sensing*, vol. 11, no. 7, pp. 1119–1144, 1990.

[40] A. Mavrovic, A. Roy, A. Royer, B. Filali, F. Boone, C. Pappas, and O. Sonnentag, "Dielectric characterization of vegetation at L band using an open-ended coaxial probe," *Geoscientific Instrumentation, Methods and Data Systems*, vol. 7, no. 3, pp. 195–208, 2018.

[41] M. A. El-Rayes and F. T. Ulaby, "Microwave dielectric spectrum of vegetation-part I: Experimental observations," *IEEE Transactions on Geoscience and Remote Sensing*, vol. GE-25, no. 5, pp. 541–549, 1987.

[42] H. Hänninen, *Boreal and Temperate Trees in a Changing Climate: Modelling the Ecophysiology of Seasonality*. Springer Science & Business Media, Dordrech, 2016, vol. 3.
[43] C. Mätzler and U. Wegmüller, "Dielectric properties of freshwater ice at microwave frequencies," *Journal of Physics D: Applied Physics*, vol. 20, no. 12, pp. 1623–1630, 1987.
[44] G. Hufford, "A model for the complex permittivity of ice at frequencies below 1 THz," *International Journal of Infrared and Millimeter Waves*, vol. 12, no. 7, pp. 677–682, 1991.
[45] J. P. Sparks, G. S. Campbell, and A. R. Black, "Water content, hydraulic conductivity, and ice formation in winter stems of pinus contorta: A TDR case study," *Oecologia*, vol. 127, no. 4, pp. 468–475, 2001.
[46] G. I. Torgovnikov, *Dielectric properties of wood and wood-based materials*. Springer-Verlag, 1993.
[47] R. Zweifel and R. Häsler, "Frost-induced reversible shrinkage of bark of mature sub alpine conifers," *Agricultural and Forest Meteorology*, vol. 102, no. 4, pp. 213–222, 2000.
[48] U. Wegmüller, "The effect of freezing and thawing on the microwave signatures of bare soil," *Remote Sensing of Environment*, vol. 33, no. 2, pp. 123–135, 1990.
[49] G. Bonan, *Climate Change and Terrestrial Ecosystem Modeling*. Cambridge University Press, Cambridge, UK, 2019.
[50] J. C. Forbes and R. D. Watson, *Plants in Agriculture*. Cambridge University Press, Cambridge, 1996.
[51] J. Čermák, J. Kučera, W. L. Bauerle, N. Phillips, and T. M. Hinckley, "Tree water storage and its diurnal dynamics related to sap flow and changes in stem volume in old-growth Douglas-fir trees," *Tree physiology*, vol. 27, no. 2, pp. 181–198, 2007.
[52] K. C. McDonald, R. Zimmermann, and J. S. Kimball, "Diurnal and spatial variation of xylem dielectric constant in Norway spruce (Picea abies [L.] Karst.) as related to microclimate, xylem sap flow, and xylem chemistry," *IEEE Transactions on Geoscience and Remote Sensing*, vol. 40, no. 9, pp. 2063–2082, 2002.
[53] M. Watanabe, T. Motohka, T. Shiraishi, R. B. Thapa, C. Yonezawa, K. Nakamura, and M. Shimada, "Multitemporal fluctuations in L-band backscatter from a Japanese forest," *IEEE Transactions on Geoscience and Remote Sensing*, vol. 53, no. 11, pp. 5799–5813, 2015.
[54] T. Chiu and K. Sarabandi, "Electromagnetic scattering interaction between a dielectric cylinder and a slightly rough surface," *IEEE Transactions on Antennas and Propagation*, vol. 47, no. 5, pp. 902–913, 1999.
[55] G. Toole and S. Tool, *New Understanding Biology for Advanced Level*, 4th ed. Nelson Thornes Ltd, Cheltenham, 1999.
[56] F. A. Daudet, X. Le Roux, H. Sinoquet, and B. Adam, "Wind speed and leaf boundary layer conductance variation within tree crown consequences on leaf-to-atmosphere coupling and tree functions," *Agricultural and Forest Meteorology*, vol. 97, no. 3, pp. 171–185, 1999.
[57] C. R. Chu, C.-I. Hsieh, S.-Y. Wu, and N. G. Phillips, "Transient response of sap flow to wind speed," *Journal of Experimental Botany*, vol. 60, no. 1, pp. 249–255, 2009.
[58] N. G. Phillips, R. Oren, J. Licata, and S. Linder, "Time series diagnosis of tree hydraulic characteristics," *Tree Physiology*, vol. 24, no. 8, pp. 879–890, 2004.
[59] F. C. Meinzer, S. A. James, G. Goldstein, and D. Woodruff, "Whole-tree water transport scales with sapwood capacitance in tropical forest canopy trees," *Plant, Cell and Environment*, vol. 26, no. 7, pp. 1147–1155, 2003.
[60] M. W. Long, *Radar reflectivity of land and sea*, 3rd ed. Artech House, Boston, 2001.
[61] R. Gall, W. Landolt, P. Schleppi, V. Michellod, and J. Bucher, "Water content and bark thickness of Norway spruce (Picea abies) stems: phloem water capacitance and xylem sap flow," *Tree Physiology*, vol. 22, no. 9, pp. 613–623, 2002.

Albert R. Monteith (S'09) received the M.Sc. degree in electrical engineering from Chalmers University of Technology, Gothenburg, Sweden in 2015. He is currently working toward the Ph.D. degree at the Department of Space, Earth and Environment. His main research interests lie in the temporal aspects of radar remote sensing of forests.

Lars M. H. Ulander (S'86-M'90-SM'04-F'17) received the M.Sc. degree in engineering physics and the Ph.D. degree in electrical and computer engineering from Chalmers University of Technology, Gothenburg, Sweden, in 1985 and 1991, respectively. Since 1995, he has been with the Swedish Defence Research Agency (FOI), where he is the Director of Research in Radar Signal Processing and leads the research on very high frequency/ultrahigh frequency band radar. Since 2014, he has been a Professor in radar remote sensing with Chalmers University of Technology. He is the author or coauthor of over 300 professional publications, of which more than 60 are in peer-reviewed scientific journals. He is the holder of five patents. His research interests include synthetic aperture radar, electromagnetic scattering models, and remote sensing applications.